amplification of the amplitude of basilar membrane vibration, i.e., cochlear amplification, leading to refinement of the sensitivity, dynamic range and frequency selectivity of mammalian hearing.

To understand the active mechanism of this hearing system, knowledge of the mechanical properties of OHCs is required since such properties are essential to the overall behavior of the organ of Corti in the cochlea. Intensive research seeking to elucidate such properties has been conducted using various kinds of experimental techniques. Zenner et al. reported the axial stiffness of the OHC using cell capillaries [7]. Employing calibrated glass fibers, Hallworth reported the axial compliance [8] and Ulfendahl et al. revealed that the axial stiffness is lower than the transverse stiffness of the OHC [9]. Tolomeo et al. applied glass pipettes for three-point bending measurements and obtained the axial stiffness of the OHC [10]. Oghalai et al. characterized the stiffness of the lateral wall of the OHC by a micropipette aspiration technique [11], and Bata et al. subsequently reported such stiffness using a similar technique [12]. Using flexible vibration fibers, He and Dallos measured the dynamic stiffness of the OHC, namely, the decrease in the axial stiffness of the cell due to depolarization and its increase due to hyperpolarization [13]. These reports addressed the whole-cell stiffness rather than the local mechanical properties of the OHC lateral wall. Sugawara et al. elucidated Young's modulus of the isolated OHC [14] and that of the inner hair cells and other cells in the organ of Corti [15] by atomic force microscopy (AFM). Recently, Zelenskaya et al. reported the viscoelastic properties of the OHC lateral wall as well as its stiffness properties as observed by AFM [16].

Mice are one of the most widely employed research animals since they have several advantages as experimental animal models. One such advantage is that many types of inbred strains, each of which possesses a gene that causes physiologically interesting characteristics, have been developed. It has also become possible to produce a variety of new types of transgenic and knockout mice using genetic-engineering techniques. With the availability of specific mice, mice have become a powerful tool for genetic research. Secondly, since there is a high homology between mouse and human genomes, in some cases, an orthologous gene is involved in the same disease, including hearing impairment, in the two species. The genomic approach using mice is thus feasible for studying human diseases. Thirdly, in 2002, the full-length mouse complementary DNA sequences were revealed by the FANTOM Consortium and the RIKEN Genome Exploration Research Group Phase I & II Team [17], making mice the experimental vertebrate with the best characterized genome to date. Thus, auditory research on mice can possibly lead to findings pertinent to not only basic but also clinical research on hearing. However, mice are seldom used in hearing research. Experiments using hearing organ tissues and/or cells, for example, are mostly limited to guinea pigs because the inner ear of guinea pigs is relatively large compared with its body weight, and thus preparation of the cells is easy. Moreover, in mice, the OHCs in the hearing organ are small and susceptible to external stimuli, and their connections with the cells are tight. Thus, isolation of OHCs is difficult. Hence, the mechanical properties of mouse OHCs have not yet been clarified.

In the present study, therefore, to establish indicators of the mechanical properties of OHCs in mice, isolation of OHCs from mice was attempted and the local mechanical properties of mouse OHCs were measured by AFM.

2. Materials and methods

2.1. Cell preparation

CBA/JNCrj strain male mice aged 10–12 weeks (25–30 g) were used. Animals were decapitated and their bullae were detached and kept in a tissue culture medium (Leibovitz's L-15, Invitrogen, Carlsbad, CA) at 4 °C, which had been adjusted to pH 7.3 and 331 mOsm. Cochleae were dissected out from the bullae and transferred into another tissue culture medium. The bony shell covering the cochlea was then removed from the oval window toward the apex by an angled pick with sharpened tip, and both the basilar membrane and the organ of Corti were simultaneously unwrapped from the basal end of the modiolus toward its apical end with forceps. Dissected coiled tissue was then severed into two pieces, i.e., the apical turn and the basal turn, and only the apical turn was used as a specimen in this study since the cells located at the basal turn of the organ of Corti are vulnerable to external stimuli and thus had possibly been destroyed when the coiled tissue was dissected from the cochlea. The tissue was then transferred to an enzymatic digestion medium which contained 1 ml of the culture medium and 1 mg of type IV collagenase (Sigma–Aldrich, St. Louis, MO). This digestion medium had been prepared before dissection and maintained at 37 °C inside an incubator. After incubation for 15 min with the enzymatic digestion medium, the tissue was transferred into an enzyme-free culture medium in glass-bottomed dishes, the glass surface of which was coated with poly-D-lysine (MatTek, Ashland, MA). Solitary OHCs were isolated by gentle trituration of the coiled tissue in that medium with a 200-μl pipette and then left at rest for a few minutes to allow attachment of the isolated cells to the bottom of the dish. For the subsequent AFM measurement, the cells showing no obvious signs of deterioration such as shrinkage, swelling and/or translocation of the nucleus were selected and measurement was carried out within 1 h after the isolation of OHCs from the organ of Corti. All experiments were performed at room temperature.

The care and use of the animals in this study were approved by the Institutional Animal Care and Use Committee of Tohoku University, Sendai, Japan.

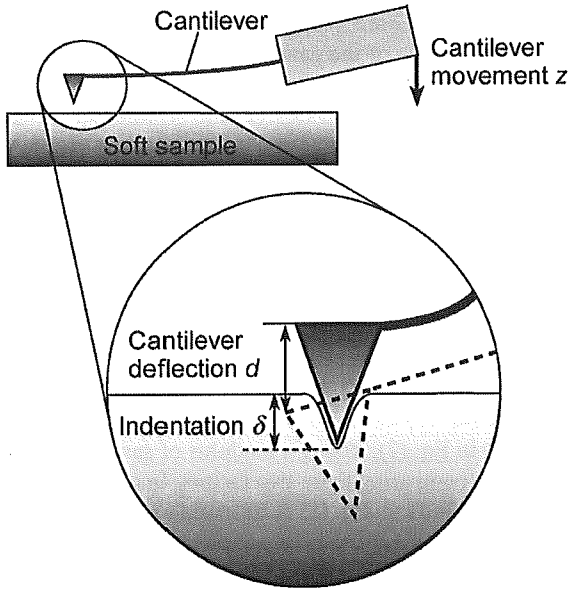

Fig. 1. A schema of the cantilever on a soft sample. When the tip of the cantilever touches the soft sample, the cantilever starts to deflect and then the deflection of the cantilever is optically detected by a laser system. By this measurement, the relationship between the movement of the cantilever z driven by a piezoelectric scanner and the cantilever deflection d was obtained.

2.2. *Atomic force microscopy*

An AFM (NVB100, Olympus, Tokyo, Japan) was used for the experiments. As the AFM unit is mounted on an inverted optical microscope, positioning of the tip above the cells is easy. V-shaped silicon nitride cantilevers (OMCL-TR400PSA-2, Olympus, Tokyo, Japan) with a pyramidal tip and a spring constant of 0.08 N/m were used. The typical radius of the curvature of the tip was less than 20 nm. Fig. 1 depicts the principal of an indentation test using the AFM. When the cantilever is moved by a piezoelectric scanner and the tip of the cantilever comes in contact with the sample, the cantilever starts to deflect, such deflection being optically detected by a laser system, which is composed of a laser, a mirror and a photodiode array. Due to this measurement, the relationship between the movement of the cantilever z driven by the piezoelectric scanner and the cantilever deflection d was obtained. This obtained curve is termed "force curve" because the force applied to the sample can be calculated by multiplying the cantilever deflection d by the spring constant of the cantilever. In each measurement, the hysteresis between two force curves, i.e., the curve obtained when the tip pushes against the sample and the curve obtained when the tip retracts from the sample, was ascertained. Because the deviations of the curves were confirmed to be negligible, the sample was kept elastic during the measurement. Fig. 2 shows an OHC isolated

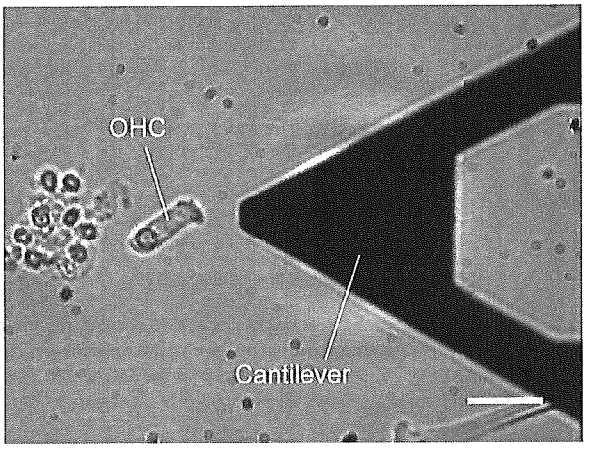

Fig. 2. Photomicrograph of an isolated OHC and the cantilever. The OHC was dissected from the apical turn of the cochlea in mice. Scale bar is 20 μm.

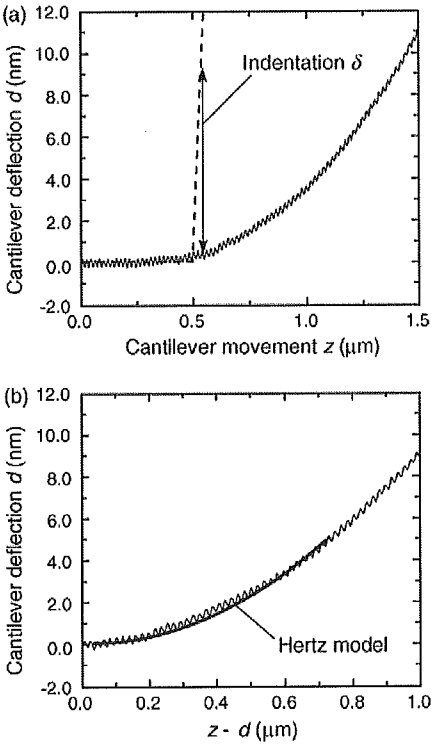

Fig. 3. Measurement data of cantilever deflection. (a) Relationship between the cantilever deflection d and cantilever movement z, i.e., force curve, obtained from both a hard sample (substrate) and a soft sample (OHC). (- - - -), hard sample; (—), soft sample. In the case of the hard sample, the cantilever deflection remains steady at zero until the cantilever touches the sample, at which time it rises proportionately with the increase in the cantilever movement. The vertical arrow shows the indentation δ, i.e., the difference between the cantilever deflection of the hard sample and that of the soft sample. (b) Relationship between the cantilever deflection d and the difference between the cantilever movement z and cantilever deflection d, i.e., $(z - d)$. The thin line shows the experimental data. The thick line represents the square regression line fitted by Eq. (5).

from the apical turn of the mouse cochlea and the cantilever.

2.3. Analysis of force curves

Examples of force curves obtained from both hard (substrate) and soft (OHC) samples are shown in Fig. 3(a). In the case of the hard sample, the cantilever deflection d remains steady at zero until the cantilever touches the sample, at which time it rises proportionately with the increase in the cantilever movement z. Regarding the case of the soft sample, the cantilever deflection d increases gradually after the cantilever touches the sample since the tip of the cantilever indents the sample; however, distinguishing the contact point between the sample and the tip of the cantilever is difficult. Thus, the contact point was numerically determined as described previously [15]. Assuming that the contact point is (z_0, d_0), the cantilever movement and the cantilever deflection after the cantilever contacts the sample, namely, post-contact cantilever movement z' and post-contact cantilever deflection d', are written as follows:

$$z' = z - z_0 \tag{1}$$

$$d' = d - d_0 \tag{2}$$

As the difference between the post-contact cantilever movement z' and the post-contact cantilever deflection d' indicates the sample indentation, the indentation δ is given by

$$\delta = z' - d' \tag{3}$$

Substituting Eqs. (1) and (2) into Eq. (3), the indentation δ is obtained as follows:

$$\delta = z' - d' = (z - z_0) - (d - d_0) \tag{4}$$

Fig. 3(b) shows the relationship between the cantilever deflection d and the difference between the cantilever movement z and the cantilever deflection d, i.e., $(z - d)$, which is obtained from Fig. 3(a). The curve in this figure is fitted with a square regression line, which is given by

$$d = a\{(z - d) - b\}^2 + c \tag{5}$$

The parameters a, b and c are obtained by the least squares method, in which a is the slope of the curve and represents the elastic properties of the sample; that is, the harder the sample, the greater the deflection of the cantilever, resulting in a larger value of slope a. When samples are elastic, isotropic, homogeneous and semi-infinite, and the indentation tip is rigid and conical, the Hertz model, which describes the elastic response of such subjects indented by the tip, can be applied to the measurement data. According to the Hertz model, the relationship between the post-contact cantilever deflection d' and the indentation δ is defined as follows:

$$d' = \{2E \tan\alpha / \pi k(1 - \nu^2)\}\delta^2 \tag{6}$$

where E, α, k and ν are Young's modulus of the sample, the half-opening angle of the cantilever, the spring constant of the cantilever and Poisson's ratio of the sample, respectively [18,19]. The substitution of Eqs. (2) and (4) into Eq. (6) leads to the following equation:

$$d = \{2E \tan\alpha / \pi k(1 - \nu^2)\}\{(z - d) - (z_0 - d_0)\}^2 + d_0 \tag{7}$$

In this study, the half-opening angle and the spring constant of the cantilever were 17° and 0.08 N/m, respectively. Poisson's ratio was assumed to be 0.499 because the samples were biomaterials, i.e., incompressible materials. Since slope a in Eq. (5) corresponds to the coefficient $2E \tan\alpha / \pi k(1 - \nu^2)$ in Eq. (7), Young's modulus of sample E can be obtained by comparing these two factors. In addition, as the parameters b and c in Eq. (5) correspond to $(z_0 - d_0)$ and d_0 in Eq. (7), respectively, the contact point (z_0, d_0) is simultaneously determined.

3. Results

3.1. Location-dependent variance of mechanical properties

Mechanical properties of the OHC in the apical turn of the cochlea were measured at various points along the longitudinal axis of the OHC. In this measurement, since the

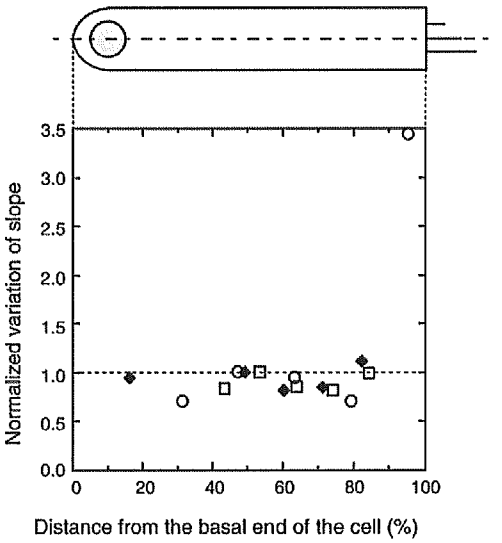

Fig. 4. Variance of the mechanical properties of OHCs along the longitudinal axis. The vertical axis represents the slope of the square regression line at the point of measurement divided by that in the middle part of the cells, and the horizontal axis shows the percentage of the distance of each measurement point from the basal end of the OHC, i.e., positions of the basal and apical ends along the cell axis are represented as 0% and 100%, respectively. The different symbols indicate the data obtained from different cells ($n = 3$). The inset represents the measurement position on the cell.

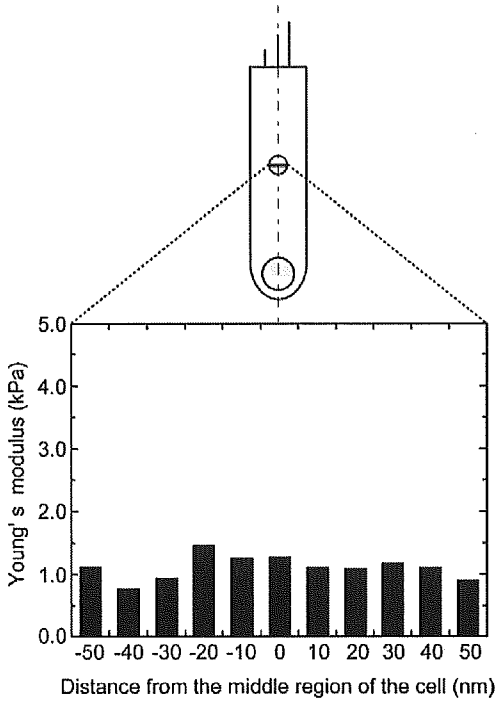

Fig. 5. Distribution of the mechanical properties of an OHC along the circumferential direction. The vertical axis represents Young's modulus and the horizontal axis shows the distance from the middle region of the measured OHC. Measurements were performed at 11 points at intervals of 10 nm. The mean and standard deviation of Young's modulus were 1.1 ± 0.19 kPa. The inset represents the measurement position on the cell.

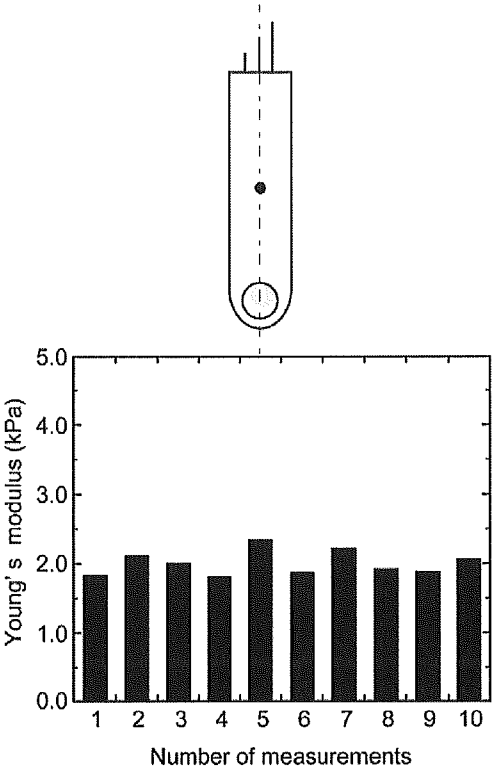

Fig. 6. Young's modulus obtained 10 times at one point in the middle region of the OHC. Young's modulus of OHCs obtained from the apical turn of the cochlea was measured 10 times at one point in the middle region of the OHC. The mean and standard deviation of Young's modulus were 2.0 ± 0.18 kPa. The inset represents the measurement position on the cell.

surface profile of the apical region of the OHC could not be regarded as semi-infinite in extent, the obtained data could not be analyzed by the Hertz model. The relationships between the cantilever deflection and the indentation of the OHC were therefore measured and the slopes of the square regression lines fitted to these relationships were obtained. Fig. 4 shows the relationship between the slope and the distance from the basal end of the OHC ($n = 3$). The horizontal axis represents the percentage of the distance of each measurement point from the basal end of the OHC, i.e., positions of the basal and apical ends along the cell axis are represented as 0% and 100%, respectively. The vertical axis shows the normalized variation of the slope, i.e., the value of the slope at each point divided by that in the middle part of the cell. From this figure, it can be seen that there was no significant difference in the mechanical properties in the region between 10% and 90% from the basal end of the cell. Hence, all measurements in the following experiments were conducted in the middle region of the OHC.

As shown in Fig. 5, variance of mechanical properties according to the location in the circumferential direction was evaluated. Measurements were performed in the middle region of an apical turn OHC at 11 points at intervals of 10 nm in the circumferential direction. The mean and standard deviation of Young's modulus were 1.1 ± 0.19 kPa. Variance of mechanical properties due to the repeated measurement at one point was then assessed as shown in Fig. 6. When Young's modulus was measured 10 times at one point in the middle region of the OHC, the mean and standard deviation of Young's modulus were 2.0 ± 0.18 kPa. No significant difference was seen between the variance of Young's modulus obtained from different points along the circumferential direction and that obtained from the repeated measurement. These results imply that the variance of Young's modulus obtained for each cell is due to repetition of the measurement rather than the location of the measurement point. Thus, to reduce this variance of Young's modulus and to take the limited measurable time of this experiment into account, force curves were obtained at one point, i.e., the central part of the middle region of the OHC, and the mean value of four Young's moduli measured at that point were defined as Young's modulus of the OHC.

3.2. Local mechanical properties of mouse outer hair cells

The relationship between Young's modulus of the mouse OHCs in the apical turn and the cell length ($n = 10$) is shown in Fig. 7. Lengths of the apical turn OHCs ranged from 15.7 to 21.3 μm and their Young's moduli ranged from 1.3 to

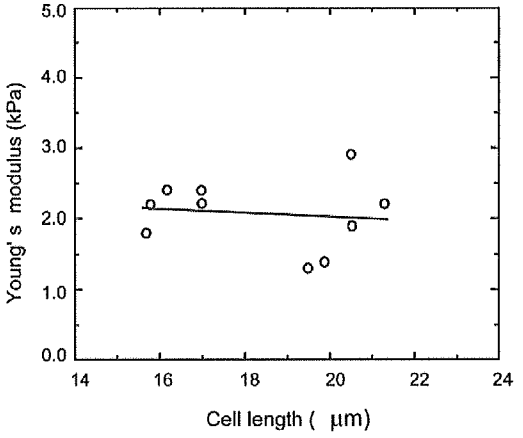

Fig. 7. Relationship between Young's modulus and the length of OHCs. Young's modulus and the cell length of OHCs ranged from 1.3 to 2.9 kPa and from 15.7 to 21.3 μm, respectively ($n = 10$). The regression line is given by $y = -0.025x + 2.5$ ($r = -0.11$). No significant correlation was observed between Young's modulus and the cell length.

2.9 kPa. The mean and standard deviation of Young's moduli of the apical turn OHCs were 2.1 ± 0.5 kPa. The regression line is given by $y = -0.025x + 2.5$ and the correlation coefficient r is -0.11. Thus, regarding OHCs in the apical turn of the mouse cochlea, no significant correlation was observed between Young's modulus and the cell length.

4. Discussion

4.1. Preparation process of outer hair cells

To measure the mechanical properties of the isolated mouse OHCs, it is essential to obtain isolated cells which are as intact as possible. The morphology of the cells was therefore microscopically examined as an index of cell intactness, and cells were selected for experiments only if they showed no obvious deterioration such as shrinkage, swelling and/or translocation of the nucleus.

In this study, the length of the selected OHCs ranged from 15.7 to 21.3 μm as shown in Fig. 7. Keiler and Richter reported the sizes of various elements in the cochlea of different strains of mice, including CBA/CaJ strain mice, by using the hemicochlea technique, which enables direct observation of cross sections of fresh mouse cochlea [20]. According to their report, the first, second and third rows of OHCs obtained from the apical turn of the cochlea of CBA/CaJ strain mice were 22.2 ± 1.4, 20.6 ± 1.3 and 19.9 ± 1.2 μm in length, respectively, i.e., the length of OHCs in the apical turn of the cochlea range from approximately 18 to 24 μm. The length of OHCs obtained in this study was 11–15% shorter than that reported in their study. Indeed, an isolated OHC with an initial length of 24.2 μm showed a gradual shortening of the cell soma, namely, the cell decreased in length to 20.7, 20.3 and 19.3 μm at 15, 25 and 45 min after isolation, respectively.

The difference in the length of OHCs between this study and Keiler and Richter's study is possibly due to differences in sample preparation; that is, OHCs were isolated from neighboring OHCs and supporting cells with enzymatic digestion and subsequent mechanical trituration using a pipette in this study, whereas a fresh cross section of the mouse hemicochlea was used as a specimen in the previous study. In this study, enzymatic isolation was carried out using type IV collagenase. Type IV collagen is a major structural component of the extracellular matrix, i.e., the basilar membrane in the organ of Corti [21]. Therefore, the influences of the enzymatic isolation with type IV collagenase on epithelial cells, i.e., OHCs in the organ of Corti, are negligibly small, suggesting that its effect on the mechanical properties of OHCs is also negligible. Although the isolation procedures applied in this study may have resulted in inevitable shrinkage of OHCs, the length change of the cell remained within 3.1 μm (13.8%), even though 45 min elapsed after isolation. Furthermore, cell morphology was microscopically fine without swelling and/or translocation of the nucleus. In this study, therefore, AFM measurement was deemed to be applicable to the isolated OHCs.

4.2. Atomic force microscopic analysis of Young's modulus of outer hair cells

Regarding the mechanical properties of OHCs, there have been various reports [7–13]. Recently, the mechanical properties of the sensory and supporting cells in the organ of Corti have been studied by AFM [14–16]. When Young's modulus of a sample is measured by AFM, the sample must be elastic, isotropic, homogenous and semi-infinite to accurately estimate Young's modulus by using a proper mathematical model, i.e., the Hertz model. In the present study, since no hysteresis was shown in the force curves between approach to and retraction from the sample, the sample was assumed to be elastic. Regarding the lateral wall of the OHC, it is considered to be orthotropic because of the existence of the actin-spectrin cortical lattice [22,23]. However, the OHC can be assumed to be isotropic when the indentation depth of the cell by the AFM tip is sufficiently large compared with the OHC diameter because Young's modulus measured by that means reflects the total of the orthotropic lateral wall and the isotropic cytoplasm of the cell rather than only the orthotropic lateral wall since the thickness of the lateral wall of the OHC is only several tens of nanometers [14]. In the present study, the diameter of the isolated mouse OHC was approximately 7 μm and the indentation depth of the cell by the cantilever tip was up to 1 μm. Thus, the sample was assumed to be isotropic. In addition, since Young's modulus was measured at the central part of the middle region of the OHC, where there are no prominent organelles such as the nucleus and endoplasmic

reticulum, the sample was assumed to be homogeneous. Moreover, when the radius of curvature of the indentation tip is sufficiently smaller than the thickness of the sample, the sample can be regarded as semi-infinite [24]. In this study, since the radius of the curvature of the cantilever tip was less than 20 nm, the semi-infinite sample assumption was satisfied. Thus, all assumptions with regard to application of the Hertz model are appropriate.

4.3. Difference in mechanical properties of OHCs between guinea pigs and mice

Although the stiffness of the guinea pig OHCs has been measured in many studies, the reported values vary from 0.147 to 25 mN/m depending on the measurements [7–10,13,14,16,25,26]. Therefore, in the present study, we compared the stiffness of the mouse OHCs with that of the guinea pig OHCs reported by the previous study [14] since the applied experimental method is identical to that of this study, i.e., an indentation test using an AFM.

Fig. 8 shows the relationship between Young's modulus and the length of the OHC obtained from mice in this study and such relationship obtained from guinea pigs investigated by Sugawara et al. [14]. As shown in this figure, Young's modulus of the mouse OHC in the apical turn of the cochlea had about the same value as that of the guinea pig OHC in the apical turn of the cochlea. The reason why the apical turn mouse OHCs had Young's moduli similar to the apical turn guinea pig OHCs is unknown. In general, Young's modulus depends only on material, not on shape. Thus, one possible reason for this similarity is the same morphology of the lateral wall of the OHC between mice and guinea pigs. However, there is a difference in subsurface-cisternal morphology between mice and guinea pigs; that is, the mouse OHC has only one layer of the subsurface cisternae (SSC), whereas the guinea pig OHC has a number of such layers [27,28]. Oghalai et al. reported that most of the lateral wall's resistance to local bending is realized by the existence of both the cortical lattice (CL) and the SSC [11]. Although to what degree the SSC contribute to OHC Young's modulus is unknown, fewer SSC layers in the mouse OHC probably resulted in Young's modulus of the mouse OHC being smaller than that of the guinea pig OHC. Based on these considerations, about the same values of Young's modulus between the mouse and guinea pig apical turn OHC imply that the morphology of the CL in the mouse OHC may also be different from that in the guinea pig OHC.

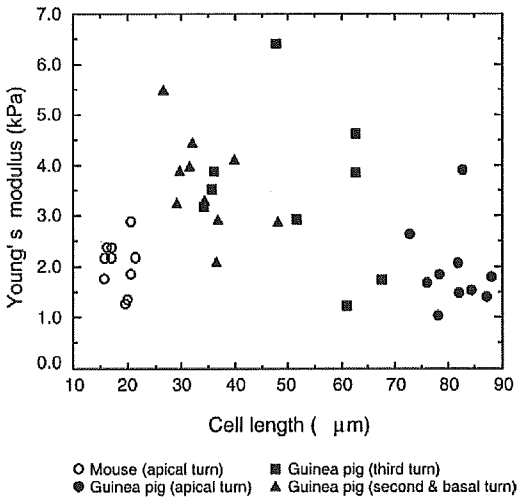

Fig. 8. Relationship between Young's modulus and the length of OHCs. Open circles represent OHCs obtained from the apical turn of the mouse cochlea in this study. Filled circles, filled squares and filled triangles represent OHCs obtained from the apical turn, the third turn and the second and basal turns of the guinea pig cochlea, respectively, as reported by Sugawara et al. [14]. Young's modulus of the OHC obtained from the apical turn of the mouse cochlea tended to be smaller and greater than those obtained from the basal turn and the apical turn of the guinea pig cochlea, respectively.

Focusing on the stiffness of the OHC, it can be evaluated from its Young's modulus by applying a simple one-dimensional model of the OHC as described previously [14]. Since isolated outer hair cells in vitro have a different condition in mechanical coupling compared with those in vivo, i.e., OHCs in vivo are connected with other OHCs, pillars, Deiters' cells, the extracellular matrix, the efferent system, etc., there is a possibility that the stiffness of OHCs in vitro differ from that of those in vivo. It has been reported that the motion of the basilar membrane included not only the AC component but also DC offset [29]. At a characteristic frequency region, the basilar membrane was displaced by about 0.2 nm toward the scala vestibuli. This compression may affect the mechanical properties of OHCs. However, the change of the OHC stiffness may be negligibly small because the 0.2-nm contraction of the OHC soma may induce a stiffness change in OHCs of only about 0.001% [13]. Assuming the cylindrical shape and homogeneity of the OHC, the stiffness of the OHC k_{cell} is shown by the following equation:

$$k_{cell} = \pi R^2 E / L \tag{8}$$

where R and L indicate the radius and length of the OHC, respectively. Derived from Eq. (8), the stiffness of the OHC in the apical turn of the mouse cochlea was estimated to be 4.4 ± 1.2 mN/m ($n = 10$), as shown in Table 1. Also shown is its Young's modulus measured in this study, as well as Young's modulus and the stiffness of the guinea pig OHC reported previously [14]. Comparing the data of the mouse OHC in the apical turn of the cochlea with those of the guinea pig OHC in the apical turn, although Young's modulus of the mouse OHC was roughly the same as that of the guinea pig OHC, the stiffness of the former is about two times greater than that of the latter.

In a general sense, the basilar membrane becomes wider and thinner with distance along the cochlea from base to apex, resulting in the graduation of its stiffness along the cochlear partition. Because of this stiffness gradient, traveling waves occur on the basilar membrane and thus

Table 1
Length, Young's modulus and stiffness of the OHC in guinea pigs and mice

Animal	Location	Cell length (μm)	Young's modulus (kPa)	Stiffness (mN/m)	Reference
Mouse	Apical turn	18.3 ± 2.2	2.1 ± 0.5	4.4 ± 1.2	This study
Guinea pig	Apical turn	81.2 ± 4.8	2.0 ± 0.81	2.0 ± 0.8	Sugawara et al. [14]
Guinea pig	Basal and second turns	34.7 ± 6.2	3.7 ± 0.96	8.7 ± 3.4	Sugawara et al. [14]

realize the frequency selectivity of mammalian hearing. Although such basic structure of the basilar membrane is conserved among mammals, the difference in the size of the basilar membrane between mice and guinea pigs has to be taken into account when the stiffness of the basilar membrane is discussed. As the longitudinal stiffness of the basilar membrane has been observed to be much smaller than the transverse stiffness in a fresh preparation [30], the basilar membrane can be represented as a series of elastic beams. Thus, when the uncoiled basilar membrane is divided at intervals of δl along the longitudinal axis of the cochlea as shown in Fig. 9, the equivalent stiffness of each beam with width w and thickness t is given by

$$K = 48EI/w^3 \tag{9}$$

where E is Young's modulus, and I is the moment of inertia of the cross-sectional area which is given by

$$I = \delta l t^3/12 \tag{10}$$

Substituting Eq. (10) into Eq. (9), the equivalent stiffness of each beam K is obtained as follows:

$$K = 4E\delta l t^3/w^3 \tag{11}$$

The reported values of the width and the thickness of the basilar membrane at the apical turn of the cochlea in mice are about 164 and 8.7 μm, respectively [20], and those in guinea pigs are about 220 and 7 μm, respectively [31]. Substituting the data of the basilar membrane width and thickness of mice and guinea pigs into Eq. (11), the equivalent stiffness of the basilar membrane per unit length, i.e., $\delta l = 1.0$ μm, in mice and that in guinea pigs is calculated to be $(6.0 \times 10^{-10})E$ and $(1.3 \times 10^{-10})E$ N/m, respectively. These results indicate that the basilar membrane at the apical turn of the cochlea in mice is about 4.6 times stiffer than that in guinea pigs if Young's modulus of the basilar membrane in mice is assumed to be the same as that in guinea pigs.

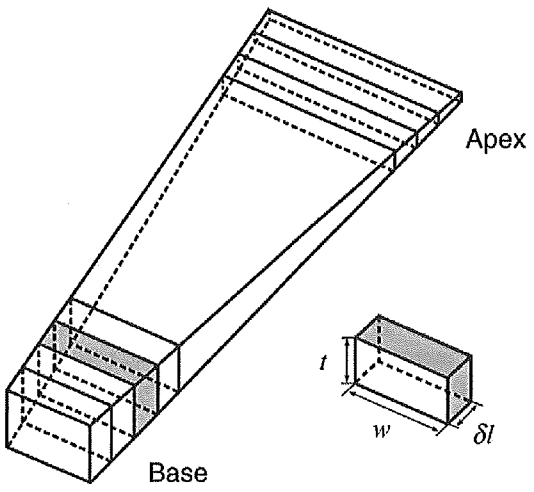

Fig. 9. Uncoiled basilar membrane represented by a series of elastic beams. The uncoiled basilar membrane is divided at intervals of δl. The width and the thickness of each beam are w and t, respectively.

The high sensitivity and sharp frequency tuning of the cochlea is realized by amplification of the basilar membrane vibration. The origin of this cochlear amplification is the force to which the basilar membrane is subjected, such force being generated by OHCs due to their electromotility. Thus, the stiffer the basilar membrane, the greater the force which must be generated by OHCs to realize the displacement of the basilar membrane vibration. In the case of mice, the basilar membrane at the apical turn of the cochlea is about 4.6 times stiffer than that of guinea pigs as mentioned above. Therefore, if the force generated by the apical turn mouse OHCs were the same as that of the apical turn guinea pig OHCs, not only the decrease of the amplitude of the basilar membrane vibration but also the lack of its tuning sharpness would result, leading to a loss of hearing sensitivity in each species. Our experimental study elucidated that the apical turn mouse OHCs are about 2.2 times stiffer than the apical turn guinea pig OHCs. According to Hooke's law, the force generated by elastic material is proportional to its stiffness for a given displacement. Based on these considerations, it can be reasonably concluded that the stiffer OHC in mice produces a greater force to amplify the vibration of the stiffer basilar membrane in the mouse cochlea.

5. Conclusions

In this study, the mechanical properties of outer hair cells (OHCs) in the apical turn of the cochlea of CBA/JNCrj strain mice were measured by atomic force microscopy. In conclusion, their Young's modulus and stiffness were 2.1 ± 0.5 kPa and 4.4 ± 1.2 mN/m, respectively. Young's modulus of the OHC in the apical turn of the cochlea in mice was roughly the same as that in the apical turn of the cochlea in guinea pigs; however, the stiffness of the former was about two times greater than that of the latter because the cell length of the former was shorter than that of the latter.

Acknowledgements

This work was supported by Grant-in-Aid for Scientific Research on Priority Areas 15086202 from the Ministry of Education, Culture, Sports, Science and Technology of Japan, by a Health and Labour Science Research Grant from the Ministry of Health, Labour and Welfare of Japan and by a grant from the Human Frontier Science Program to H.W., by Grants-in-Aid for Scientific Research 14770881 and 17591774 from the Ministry of Education, Culture, Sports, Science and Technology of Japan to N.Y. and by the Special Research Grant 11170012 from the Tohoku University 21st Century COE Program of the "Future Medical Engineering Based on Bio-nanotechnology" to M.M.

References

[1] Békésy GV. Experiments in hearing. New York, NY: McGraw-Hill Book Company, Inc.; 1960. pp. 452–455.
[2] Brownell WE, Bader CR, Bertrand D, de Ribaupierre Y. Evoked mechanical responses of isolated cochlear outer hair cells. Science 1985;227:194–6.
[3] Kachar B, Brownell WE, Altschuler R, Fex J. Electrokinetic shape changes of cochlear outer hair cells. Nature 1986;322:365–8.
[4] Ashmore JF. A fast motile response in guinea-pig outer hair cells: the cellular basis of the cochlear amplifier. J Physiol 1987;388:323–47.
[5] Santos-Sacchi J, Dilger JP. Whole cell currents and mechanical responses of isolated outer hair cells. Hear Res 1988;35:143–50.
[6] Canlon B, Brundin L, Flock A. Acoustic stimulation causes tonotopic alterations in the length of isolated outer hair cells from guinea pig hearing organ. Proc Natl Acad Sci USA 1988;85:7033–5.
[7] Zenner HP, Gitter AH, Rudert M, Ernst A. Stiffness, compliance, elasticity and force generation of outer hair cells. Acta Otolaryngol (Stockh) 1992;112:248–53.
[8] Hallworth R. Passive compliance and active force generation in the guinea pig outer hair cell. J Neurophysiol 1995;74:2319–28.
[9] Ulfendahl M, Chan E, McConnaughey WB, Prost-Domasky S, Elson EL. Axial and transverse stiffness measures of cochlear outer hair cells suggest a common mechanical basis. Pflügers Arch 1998;436:9–15.
[10] Tolomeo JA, Steele CR, Holley MC. Mechanical properties of the lateral cortex of mammalian auditory outer hair cells. Biophys J 1996;71:421–9.
[11] Oghalai JS, Patel AA, Nakagawa T, Brownell WE. Fluorescence-imaged microdeformation of the outer hair cell lateral wall. J Neurosci 1998;18:48–58.
[12] Bata TJ, Panyi G, Gásár R, Sziklai I. Active and passive behavior in the regulation of stiffness of the lateral wall in outer hair cells of the guinea-pig. Pflügers Arch 2003;447:328–36.
[13] He DZZ, Dallos P. Somatic stiffness of cochlear outer hair cells is voltage-dependent. Proc Natl Acad Sci USA 1999;96:8223–8.
[14] Sugawara M, Ishida Y, Wada H. Local mechanical properties of guinea pig outer hair cells measured by atomic force microscopy. Hear Res 2002;174:222–9.
[15] Sugawara M, Ishida Y, Wada H. Mechanical properties of sensory and supporting cells in the organ of Corti of the guinea pig cochlea—study by atomic force microscopy. Hear Res 2004;192:57–64.
[16] Zelenskaya A, Monvel JB, Pesen D, Radmacher M, Hoh JH, Ulfendahl M. Evidence for a highly elastic shell-core organization of cochlear outer hair cells by local membrane indentation. Biophys J 2005;88:2982–93.
[17] The FANTOM Consortium and the RIKEN Genome Exploration Research Group Phase I & II Team. Analysis of the mouse transcriptome based on functional annotation of 60, 770 full-length cDNAs. Nature 2002;420:563–73.
[18] Sneddon IN. The relation between load and penetration in the axisymmetric Boussinesq problem for a punch of arbitrary profile. Int J Eng Sci 1965;3:47–57.
[19] Wu HW, Kuhn T, Moy VT. Mechanical properties of L929 cells measured by atomic force microscopy: effects of anticytoskeletal drugs and membrane crosslinking. Scanning 1998;20:389–97.
[20] Keiler S, Richter CP. Cochlear dimensions obtained in hemicochleae of four different strains of mice: CBA/CaJ, 129/CD1, 129/SvEv and C57BL/6J. Hear Res 2001;162:91–104.
[21] Kalluri R, Gattone II VH, Hudson BG. Identification and localization of type IV collagen chains in the inner ear cochlea. Connect Tissue Res 1998;37:143–50.
[22] Sugawara M, Wada H. Analysis of elastic properties of outer hair cell wall using shell theory. Hear Res 2001;160:63–72.
[23] Wada H, Kimura K, Gomi T, Sugawara M, Katori Y, Kakehata S, et al. Imaging of the cortical cytoskeleton of guinea pig outer hair cells using atomic force microscopy. Hear Res 2004;187:51–62.
[24] Dimitriadis EK, Horkay F, Maresca J, Kachar B, Chadwick RS. Determination of elastic moduli of thin layers of soft material using the atomic force microscope. Biophys J 2002;82:2798–810.
[25] Holley MC, Ashmore JF. A cytoskeletal spring in cochlear outer hair cells. Nature 1988;335:635–7.
[26] Iwasa KH, Adachi M. Force generation in the outer hair cell of the cochlea. Biophys J 1997;73:546–55.
[27] Forge A. Structural features of the lateral walls in mammalian cochlear outer hair cells. Cell Tissue Res 1991;265:473–83.
[28] Raphael Y, Altschuler RA. Structure and innervation of the cochlea. Brain Res Bull 2003;60:397–422.
[29] LePage EL. Frequency-dependent self-induced bias of the basilar membrane and its potential for controlling sensitivity and tuning in the mammalian cochlea. J Acoust Soc Am 1987;82:139–54.
[30] Voldrich L. Mechanical properties of basilar membrane. Acta Otolaryngol (Stockh) 1978;86:331–5.
[31] Wada H, Sugawara M, Kobayashi T, Hozawa K, Takasaka T. Measurement of guinea pig basilar membrane using computer-aided three-dimensional reconstruction system. Hear Res 1998;120:1–6.

Available online at www.sciencedirect.com
SCIENCE DIRECT®
Hearing Research 205 (2005) 262–270
HEARING RESEARCH
www.elsevier.com/locate/heares

Construction of an expression system for the motor protein prestin in Chinese hamster ovary cells

Koji Iida [a], Kouhei Tsumoto [b], Katsuhisa Ikeda [c], Izumi Kumagai [b], Toshimitsu Kobayashi [d], Hiroshi Wada [a,*]

[a] *Department of Bioengineering and Robotics, Tohoku University, 6-6-01 Aoba-yama, Sendai 980-8579, Japan*
[b] *Department of Biomolecular Engineering, Tohoku University, 6-6-07 Aoba-yama, Sendai 980-8579, Japan*
[c] *Department of Otorhinolaryngology, Juntendo University School of Medicine, 2-1-1 Hongo, Bunkyo-ku, Tokyo 113-8421, Japan*
[d] *Department of Otolaryngology – Head and Neck Surgery, Tohoku University School of Medicine, 1-1 Seiryo-machi, Sendai 980-8575, Japan*

Received 23 August 2004; accepted 15 March 2005
Available online 28 April 2005

Abstract

The electromotility of outer hair cells (OHCs) is believed to be a major factor in cochlear amplification that enables the high sensitivity of hearing in mammals. This motility is thought to be based on voltage-dependent conformational changes of a motor protein embedded in the lateral wall of the OHC. In 2000, this motor protein was identified and termed prestin. To obtain knowledge on the function of prestin, research at the molecular level is necessary. For this purpose, a method of obtaining a large amount of prestin is required. In this study, an attempt was therefore made to construct an expression system for prestin. Prestin cDNA was introduced into *Escherichia coli* (*E. coli*), insect cells and Chinese hamster ovary (CHO) cells, and the expression of prestin was examined by Western blotting. As CHO cells expressed prestin well, we generated prestin-expressing cell lines using CHO cells by limiting dilution cloning. The stable expression and the activity of prestin in generated cell lines were then confirmed. Finally, to obtain prestin from these cell lines efficiently, culture conditions of the cells were examined, and it was clarified that cells should be cultured in serum-free medium and harvested around 48 h after passage.

Keywords: Outer hair cell; Prestin; Chinese hamster ovary cell; Cloning; Stable expression

1. Introduction

Mammalian hearing sensitivity relies on a mechanical amplification mechanism based on the electromotility of outer hair cells (OHCs) (Brownell et al., 1985; Kachar et al., 1986; Zenner, 1986; Ashmore, 1987; Santos-Sacchi and Dilger, 1988). This mechanism enables the high sensitivity, wide dynamic range and sharp frequency selectivity of hearing in mammals (Dallos, 1992). The molecular basis of this mechanism is thought to be voltage-dependent conformational changes of motor proteins, which are embedded in the plasma membrane of the OHC lateral wall (Forge, 1991; Huang and Santos-Sacchi, 1993).

In 2000, Zheng et al. identified the motor protein in the gerbil cochlea and termed it prestin. Since its identification, prestin has been intensively researched to elucidate the characteristic behavior of the OHCs. As a result, it has been confirmed that prestin-transfected mammalian cells show characteristic features of the

Abbreviations: OHC, outer hair cell; *E. coli*, *Escherichia coli*; CHO, Chinese hamster ovary; MBP, maltose-binding protein; GFP, green fluorescent protein

* Corresponding author. Tel.: +81 22 795 6938; fax: +81 22 795 6939.
E-mail address: wada@cc.mech.tohoku.ac.jp (H. Wada).

0378-5955/$ - see front matter © 2005 Elsevier B.V. All rights reserved.
doi:10.1016/j.heares.2005.03.027

OHC based on its motor protein, i.e., they exhibit voltage-dependent nonlinear capacitance (Zheng et al., 2000; Ludwig et al., 2001; Santos-Sacchi et al., 2001), electromotility (Zheng et al., 2000) and force generation (Ludwig et al., 2001). It has also been clarified that both the amino and carboxyl termini are located on the intracellular side (Zheng et al., 2001) and that intracellular anions act as voltage sensors of prestin (Oliver et al., 2001). In addition, Liberman et al. (2002) generated prestin knockout mice and showed that targeted deletion of prestin in mice resulted in a loss of OHC electromotility in vitro. Such deletion has also been found to result in a 40–60 dB loss of cochlear sensitivity in vivo (Wu et al., 2004).

However, the motor function of prestin still needs to be understood at the molecular level. For this purpose, a method of obtaining a large amount of prestin as material for such research is required. In this study, an attempt was therefore made to construct an expression system for prestin. Prestin cDNA was introduced into *Escherichia coli* (*E. coli*), insect cells and Chinese hamster ovary (CHO) cells, and the expression of prestin was examined by Western blotting. As CHO cells expressed prestin, stable prestin-expressing cell lines were generated using transfected CHO cells by limiting dilution cloning. The expression of prestin and the activity of prestin in the generated cell lines were then examined by immunofluorescence experiments and patch–clamp measurements, respectively. Finally, to obtain prestin from these cell lines efficiently, the optimal culture condition of the cells was considered.

2. Materials and methods

2.1. Verification of expression in cells

Escherichia coli expression vectors pET28b (Novagen, Madison, WI), pET20b (Novagen) and pMAL-c2 (New England Biolabs, Beverly, MA) were used for the *E. coli* expression system. Gerbil prestin cDNA was inserted into these vectors. The open reading frame of the prestin cDNA was fused in a frame with the His_6-tag coding sequence of the expression vector pET28b or pET20b. For this purpose, the stop codon was removed. To express prestin as a maltose-binding protein (MBP)-fusion protein, prestin cDNA was inserted into the pMAL-c2 expression vector. The *E. coli* strains BL21 and JM109 were transformed by heat shock with pET28b or pET20b and pMAL-c2 *E. coli* expression vectors containing prestin cDNA, respectively. *E. coli* transformed with pET28b or pET20b was cultured in 200 ml 2× YT medium at 28 °C, and *E. coli* transformed with pMAL-c2 was cultured in 200 ml LB medium at 37 °C. When the bacteria had grown to an optical density at 600 nm of 0.6, IPTG was added to a final concentration of 1 mM. After 2–5 h, cells were harvested and the expression of prestin in bacteria was examined by Western blotting. When pET28b or pET20b was used, the expression was examined with anti-His_6 antibody (Invitrogen, Rockville, MD), and when pMAL-c2 was used, the expression was examined with anti-MBP antibody (New England Biolabs).

To use the baculovirus expression system, the pVL1392 transfer vector (PharMingen, San Diego, CA) was employed. Prestin cDNA fused at its 3′ end to the His_6-tag coding sequence was introduced into the pVL1392 transfer vector. Linearized baculovirus DNA (BaculoGold, Pharmingen) and the constructed pVL1392 transfer vector containing the prestin cDNA were co-transfected into Sf9 insect cells using Lipofectin Reagent (Invitrogen). The recombinant baculovirus was then amplified. Sf9 cells plated onto a 35-mm plate with 2 ml of fresh medium were infected with amplified baculovirus. After incubation for 3 days, cells were harvested and the expression of prestin in Sf9 cells was examined by Western blotting with anti-His_6 antibody.

For the mammalian expression system, the pIRES-hrGFP-1a (Stratagene, La Jolla, CA) mammalian expression vector was used. The open reading frame of the prestin cDNA was fused in the frame with the FLAG-tag of the expression vector. CHO-K1 cells (provided by the Cell Resource Center for Biomedical Research, Tohoku University) were transfected with the constructed expression vector using LipofectAMINE 2000 Reagent (Invitrogen). Transfected CHO cells were cultured in RPMI-1640 medium with 10% fetal bovine serum, 100 U penicillin/ml and 100 μg streptomycin/ml at 37 °C with 5% CO_2 for 2 days, and the expression of prestin in CHO cells was then examined by Western blotting with anti-FLAG antibody (Sigma–Aldrich, St. Louis, MO).

When Western blotting was performed, cell proteins were separated on 10% SDS–polyacrylamide gel and electroblotted onto nitrocellulose membrane. After blocking with skimmed milk, membranes were incubated with the primary antibody described above. Bands were visualized using horseradish peroxidase-conjugated secondary antibody and the ECL Western blotting detection system (Amersham–Pharmacia Biotech, Buckinghamshire, UK).

2.2. Cloning of prestin-expressing CHO cells

As prestin was expressed in CHO cells, an attempt was made to generate stable prestin-expressing cell lines using CHO cells. Wild-type prestin cDNA or C-terminal FLAG-tagged prestin cDNA contained in the pIRES-hrGFP-1a mammalian expression vectors was transfected into CHO cells using LipofectAMIN 2000 Reagent. After transfection, cells were plated out at a density of one cell/well in 96-well tissue culture plates. Plates were

incubated at 37 °C with 5% CO_2. Single colonies contained in 96-well plates were scaled up. Clones with slow growth were discarded. As the pIRES-hrGFP-1a vector includes the green fluorescent protein (GFP) gene, transfected clones were chosen based on the fluorescence of GFP using a fluorescent microscope.

2.3. Immunofluorescence experiments

To confirm the expression of FLAG-tagged prestin in the generated cell lines, immunofluorescence experiments were performed. CHO cells transfected with FLAG-tagged prestin and untransfected CHO cells were fixed with 4% formaldehyde in phosphate buffer for 5 min at room temperature and washed with PBS. The samples were then incubated with skim milk and fetal bovine serum for 30 min at 37 °C. After PBS washing, cells were incubated with anti-FLAG primary antibody in PBS with 0.1% saponin solution for 1 h at 37 °C. The samples were then washed with PBS and incubated with TRITC-conjugated anti-mouse IgG secondary antibody (Sigma–Aldrich) in PBS containing 0.1% saponin solution for 30 min at 37 °C. Finally, the samples were washed with PBS, and immunofluorescence images of the samples were obtained using a confocal laser scanning microscope (LSM-GB200, Olympus, Tokyo, Japan).

2.4. Functional analysis of the generated cell lines

To confirm the activity of prestin expressed in the generated cell lines, the electrophysiological properties of these cell lines were measured. Patch pipettes for whole-cell patch–clamp recordings were pulled from glass capillaries with a puller (PP-830, Narishige). Patch pipettes had a resistance of 2–3 MΩ when filled with an internal solution composed of 140 mM KCl, 3.5 mM $MgCl_2$, 5 mM EGTA, 5 mM Hepes, 0.1 mM $CaCl_2$ and 2.5 mM Na_2ATP, adjusted to pH 7.3. The bath solution contained 145 mM NaCl, 5.8 mM KCl, 1.3 mM $CaCl_2$, 0.9 mM $MgCl_2$, 10 mM Hepes, 0.7 mM Na_2HPO_4 and 5.6 mM glucose, adjusted to pH 7.3.

The measurement system consisted of a patch amplifier (Axopatch 200B, Axon Instruments, Foster City, CA), an A/DD/A converter (Digidata 1320A, Axon Instruments), a personal computer and a function generator (WF1944, NF Electronic Instruments, Kanagawa, Japan). Measurements of cell capacitance were performed using the membrane test feature of pCLAMP 8.0 acquisition software (Axon Instruments). A test square wave (amplitude, 20 mV; period $T = 4$ ms, i.e., frequency, 250 Hz) was generated by the personal computer controlled by pCLAMP 8.0 software and applied to the cell through the amplifier. The transient current, which is caused by the test square wave, was then sampled through the amplifier. Transient current Q, current decay τ and total resistance R_t were continuously calculated by pCLAMP 8.0 software at a resolution of 25 Hz, by averaging the responses to 10 positive and 10 negative consecutive test steps, and measured values of these parameters were stored in the computer. Access resistance R_a, membrane resistance R_m and membrane capacitance C_m were then obtained by substituting Q, τ and R_t into the following equations (Huang and Santos-Sacchi, 1993):

$$R_a = \frac{R_t \tau V_c}{Q R_t + \tau V_c}, \tag{1}$$

$$R_m = R_t - R_a, \tag{2}$$

$$C_m = \left(\frac{R_t}{R_m}\right)^2 \frac{Q}{V_c}, \tag{3}$$

where V_c is a voltage step. To determine the voltage dependence of membrane capacitance, triangular voltage ramps were superimposed on the above-mentioned square test wave. This triangular voltage wave (period $T = 2$ s) was generated by the function generator and swung the cell potential from −140 to +70 mV (Frolenkov et al., 2000).

After the measurements, the membrane capacitance was plotted versus the membrane potential. The membrane capacitance was fitted to the derivative of a Boltzmann function (Santos-Sacchi, 1991)

$$C_m(V) = C_{lin} + \frac{Q_{max}}{\alpha e^{\frac{V-V_{1/2}}{\alpha}}\left(1 + e^{-\frac{V-V_{1/2}}{\alpha}}\right)^2}, \tag{4}$$

where C_{lin} is the linear capacitance, Q_{max} is the maximum charge transfer, V is the membrane potential and $V_{1/2}$ is the voltage at half-maximal charge transfer. In Eq. (4), α is the slope factor of the voltage dependence of the charge transfer and is given by

$$\alpha = kT/ze, \tag{5}$$

where k is Boltzmann's constant, T is absolute temperature, z is valence and e is electron charge. When the membrane capacitance of the cell was fitted to Eq. (4) with the correlation coefficient $R \geqslant 0.98$, the cell was defined as showing nonlinear capacitance.

2.5. Outer hair cell isolation

To compare the properties of prestin expressed in generated cell lines with those in OHCs, membrane capacitance of OHCs from guinea pigs was measured in advance. Guinea pigs weighing between 200 and 500 g were used. They were decapitated and temporal bones were removed. After the bulla had been opened, the cochlea was detached and transferred to an experimental bath. The bony shell covering the cochlea was removed and the organ of Corti was gently dissociated from the basilar membrane. The OHCs were isolated

by gently pipetting the organ of Corti after enzymatic incubation with dispase (500 U/ml). The care and use of the animals in this study were approved by the Institutional Animal Care and Use Committee of Tohoku University, Sendai, Japan.

2.6. Suspension culture of FLAG-tagged prestin-expressing CHO cells

Generally, a large number of cells can be obtained efficiently and conveniently by suspension culture (Avgerinos et al., 1990). Accordingly, FLAG-tagged prestin-expressing CHO cells, which are essentially adhesive cells, were adapted from serum supplemented medium to CHO-S-SFM II (Invitrogen) serum-free medium. They were then statically subcultured in this medium because it enables CHO cells to grow in suspension. To examine the activities of prestin, which were expressed in the cells cultured in the CHO-S-SFM II medium, the electrophysiological properties of the cells were measured using patch–clamp recordings.

To obtain prestin from the cells efficiently, the time course of the quantity of the cells and the amount of prestin per unit number of cells, i.e., expression level, were examined to consider when cells should be harvested. The quantity of the cells was evaluated by cell density, i.e., counting cell number per unit volume of culture medium with a hemocytometer every 12 h after passage. To examine the expression level of prestin, first, aliquots of 5×10^4 cells were harvested every 12 h and Western blotted with anti-FLAG primary antibody and anti-mouse IgG horseradish peroxidase-conjugated secondary antibody (New England Biolabs) after electrophoresis on a 10% SDS–polyacrylamide gel. Proteins were then visualized using the ECL Western blotting detection system and a luminescent image analyzer (LAS-1000, Fuji Film, Tokyo, Japan), and the luminescence intensity of the bands, which indicate FLAG-tagged prestin, was measured.

3. Results

3.1. Prestin expression in cells

Prestin cDNA was introduced into *E. coli*, Sf9 insect cells and CHO cells, and the expression of prestin was examined by Western blotting. Prestin has a predicted molecular weight of 81.4 kDa. The results of Western blotting used to assay the expression of prestin are shown in Fig. 1. When the *E. coli* expression system was employed, bands, which show the expression of prestin, were not detected, although three kinds of expression vectors were used for transformation. By contrast, when the baculovirus expression system was used, a band around 65 kDa and some weak bands below that were detected in transfected cells, but no band

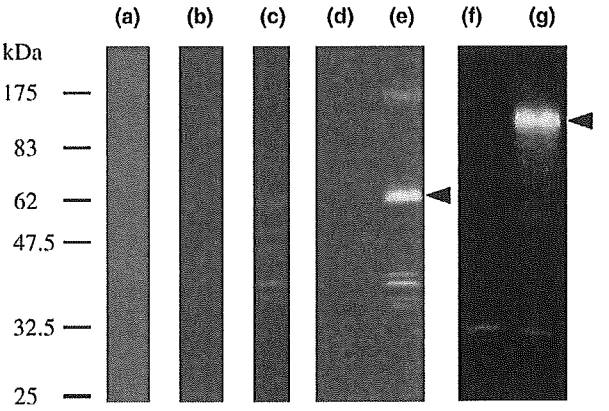

Fig. 1. Expression of prestin examined by Western blot analysis. (a) *E. coli* BL21 transformed with the pET28b vector containing prestin cDNA. (b) *E. coli* BL21 transformed with the pET20b vector containing prestin cDNA. (c) *E. coli* JM109 transformed with the pMAL-c2 vector containing prestin cDNA. (d) Untransfected Sf9 insect cells. (e) Sf9 insect cells transfected with the pVL1392 vector containing prestin cDNA. (f) Untransfected CHO cells. (g) CHO cells transfected with the pIRES-hrGFP-1a vector containing prestin cDNA. Arrows indicate the prestin bands. Bands were not detected using the *E. coli* expression system. By contrast, bands showing prestin were detected when a baculovirus expression system or a mammalian expression system was used.

was detected in untransfected cells. When the CHO cell expression system was used, a strong, broad band around 90 kDa was detected in transfected cells, and bands around 30 kDa were detected in both untransfected cells and transfected cells. These results indicate that the prestin is expressed well in CHO cells. An attempt was therefore made to construct stable prestin-expressing cell lines using transfected CHO cells.

3.2. Generation of prestin-expressing CHO cell lines

Cells were plated out into 96 wells after transfection. In the case of CHO cells transfected with wild-type prestin, 26 wells contained a single colony, the growth of 22 of them being good. In two of their clones, it was confirmed by fluorescence observation that all cells expressed GFP. In the case of CHO cells transfected with FLAG-tagged prestin, 21 wells contained a single colony, the growth of 13 of them being good. In two of their clones, it was confirmed by fluorescence observation that all cells expressed GFP. These four clones were then passaged over 40 times for 4 months, examination revealing that they retained the expression of the GFP. One of the obtained wild-type prestin-expressing cell lines and one of the FLAG-tagged prestin-expressing cell lines were then used for the following analysis.

3.3. Expression of prestin in generated cell lines

Although introduction of the expression vector and GFP expression were clarified by fluorescence

observation, the expression of prestin had not yet been elucidated. The expression of FLAG-tagged prestin in generated cells, which were subcultured for 4 months, was therefore examined by immunofluorescence experiments. Results are shown in Fig. 2. The plasma membrane of 83% of the generated cells was stained. By contrast, untransfected cells were not stained.

3.4. Activity of prestin expressed in generated cell lines

After the expression of prestin was confirmed by immunofluorescence staining, the activity of prestin expressed in the generated cell lines was examined by patch–clamp measurements. Before obtaining the electrophysiological properties of CHO cells, those of OHCs of guinea pig were measured. They exhibited bell-shaped nonlinear membrane capacitance in response to ramping of the transmembrane voltage (Fig. 3). This nonlinear membrane capacitance was well fitted to a derivative of a Boltzmann function (Eq. (4)). In a group of 11 cells, the fitting parameters of Eq. (4) were obtained as C_{lin} = 26.8 ± 3.7 pF, Q_{max} = 2.88 ± 0.65 pC, α = 28.4 ± 2.3 mV and $V_{1/2}$ = −40.1 ± 9.5 mV (mean ± SD) (Table 1).

The electrophysiological properties of wild-type prestin-expressing CHO cells and those of FLAG-tagged prestin-expressing CHO cells were then measured. The membrane capacitance versus membrane potential measured in a wild-type prestin-expressing CHO cell and that measured in a FLAG-tagged prestin-expressing CHO cell are shown in Fig. 4(a) and (b), respectively. As shown in these figures, wild-type prestin-expressing cells and FLAG-tagged prestin-expressing cells exhibited bell-shaped nonlinear membrane capacitance fitted to Eq. (4). In the case of wild-type prestin-expressing cells, 20 of 57 randomly measured cells showed nonlinear membrane capacitance, the fitting parameters of Eq. (4) being obtained as C_{lin} = 19.7 ± 4.1 pF, Q_{max} = 75.5 ± 37.3 fC, α = 38.1 ± 4.8 mV and $V_{1/2}$ = −74.8 ± 11.6 mV (mean ± SD) (Table 1). In the case of FLAG-tagged prestin-expressing cells, 19 of 53 randomly measured cells showed nonlinear membrane capacitance, the fitting parameters of Eq. (4) being obtained as C_{lin} = 24.5 ± 8.3 pF, Q_{max} = 101.3 ± 51.9 fC, α = 38.0 ± 5.5 mV and $V_{1/2}$ = −73.0 ± 12.9 mV (mean ± SD) (Table 1). By contrast, untransfected cells (n = 21) did not exhibit nonlinear membrane capacitance (Fig. 4(c)).

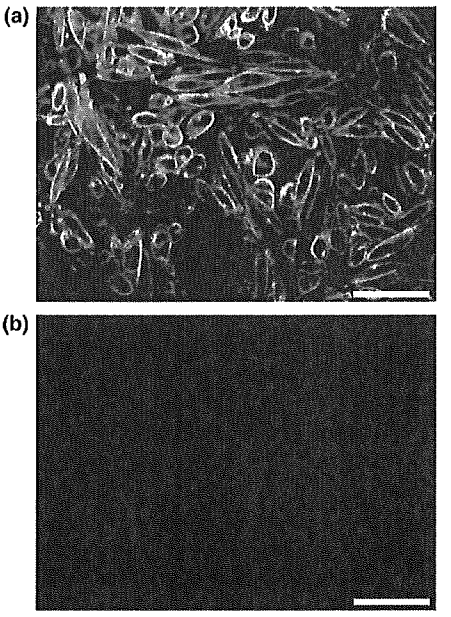

Fig. 2. Immunofluorescence images. (a) FLAG-tagged prestin-transfected CHO cell line. (b) Untransfected CHO cells. Fluorescent stains were observed in the transfected cell line after 4 months of subculture. By contrast, untransfected cells were not stained. Scale bars are 50 μm.

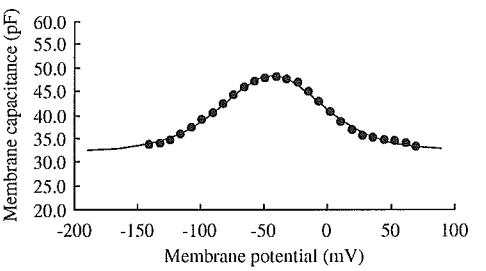

Fig. 3. Representative data of the voltage-dependent membrane capacitance of a guinea-pig OHC. Data points are fitted to Eq. (4), which is shown by the solid line. Fitting parameters are C_{lin} = 33.1 pF, Q_{max} = 2.33 pC, α = 28.0 mV and $V_{1/2}$ = −40.3 mV.

3.5. Efficient culture of FLAG-tagged prestin-expressing CHO cell line

When CHO cells which expressed FLAG-tagged prestin, the activity of which was confirmed by patch–clamp measurements, were cultured in CHO-S-SFM II medium, cells grew in suspension (Fig. 5). The electrophysiological properties of these cells were examined.

Table 1
Fitting parameters of the derivative of a Boltzmann function and charge density

	C_{lin} (pF)	Q_{max} (fC)	α (mV)	$V_{1/2}$ (mV)	Charge density (μm^{-2})
OHC (n = 11)	26.8 ± 3.7	2,878 ± 653	28.4 ± 2.3	−40.1 ± 9.5	6,830 ± 1,910
Wild-type prestin-expressing CHO cells (n = 20)	19.7 ± 4.1	75.5 ± 37.3	38.1 ± 4.8	−74.8 ± 11.6	246 ± 125
FLAG-tagged prestin-expressing CHO cells (n = 19)	24.5 ± 8.3	101.3 ± 51.9	38.0 ± 5.5	−73.0 ± 12.9	255 ± 88

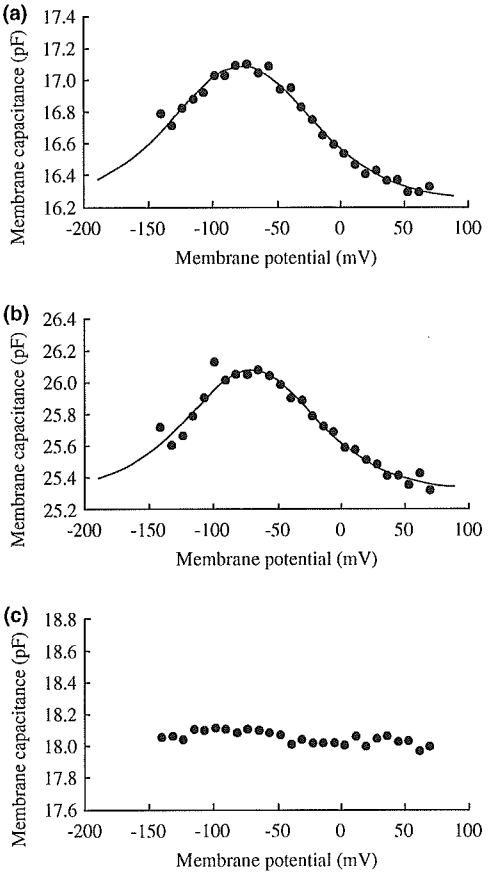

Fig. 4. Representative data of the measured membrane capacitance versus membrane potential. (a) Membrane capacitance of a wild-type prestin-expressing CHO cell. Data points are fitted to Eq. (4), which is shown by the solid line, with the following parameters: C_{lin} = 16.2 pF, Q_{max} = 127.1 fC, α = 36.8 mV and $V_{1/2}$ = −76.9 mV. (b) Membrane capacitance of a FLAG-tagged prestin-expressing CHO cell. Data points were fitted to Eq. (4), which is shown by the solid line, with the following parameters: C_{lin} = 25.3 pF, Q_{max} = 103.6 fC, α = 33.8 mV and $V_{1/2}$ = −70.4 mV. (c) Membrane capacitance of an untransfected CHO cell.

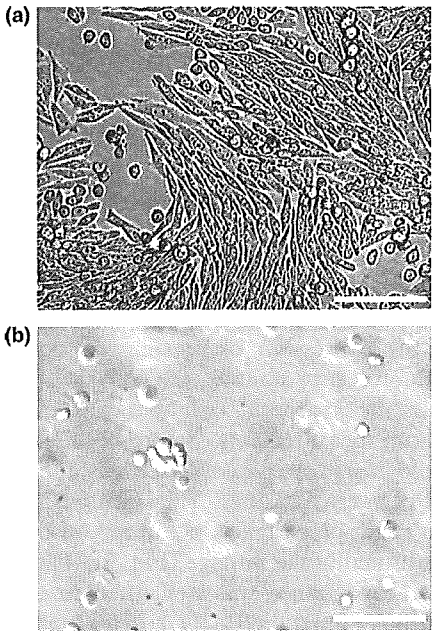

Fig. 5. Optical microscope images of FLAG-tagged prestin-expressing CHO cells. (a) Cells cultured in RPMI1640 medium containing 10% fetal bovine serum. (b) Cells cultured in CHO-S-SFM II medium. In (a), cells adhered to the culture dish and were spindle shaped. Spherical cells would be in the cell division phase. In (b), cells were suspended in the medium and were rounded. The focus plane was set above the bottom of the culture dish. Scale bars are 100 μm.

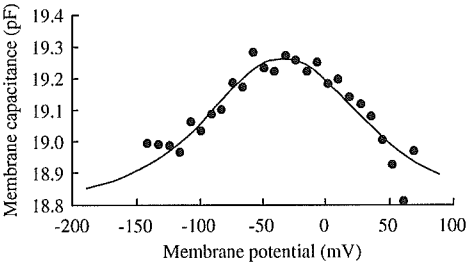

Fig. 6. Representative data of voltage dependent membrane capacitance of FLAG-tagged prestin-expressing CHO cells cultured in CHO-S-SFM II medium. Data points are fitted to Eq. (4), which is shown by the solid line. Fitting parameters are C_{lin} = 18.8 pF, Q_{max} = 70.7 fC, α = 39.8 mV and $V_{1/2}$ = −32.9 mV.

As shown in Fig. 6, when the measurements were performed at 36 h after passage, cells exhibited bell-shaped nonlinear membrane capacitance. This nonlinear membrane capacitance was fitted to Eq. (4), fitting parameters being C_{lin} = 18.8 pF, Q_{max} = 70.7 fC, α = 39.8 mV and $V_{1/2}$ = −32.9 mV. Nonlinear membrane capacitance similar to that shown by the data in Fig. 6 was observed at different points of time after passage.

Fig. 7 shows the time course of the cell density determined with a hemocytometer every 12 h (n = 4). It increased from 3×10^5 to 1×10^6 cells/ml and became saturated at 60 h after passage. The expression level of FLAG-tagged prestin every 12 h was assayed by Western blotting (Fig. 8). The bands around 90 kDa indicate prestin (Fig. 8(a)). The expression levels of prestin were evaluated based on the luminescence intensity of these bands, and the relative expression levels to the expression level in the cells cultured 12 h after passage were plotted against time (Fig. 8(b)). The expression level reached a maximum at 24 h after passage and then decreased.

4. Discussion

To obtain a large amount of prestin, we attempted to construct an expression system for prestin using *E. coli*, insect cells and CHO cells. Neither *E. coli* nor insect cells expressed prestin well. By contrast, prestin was found to

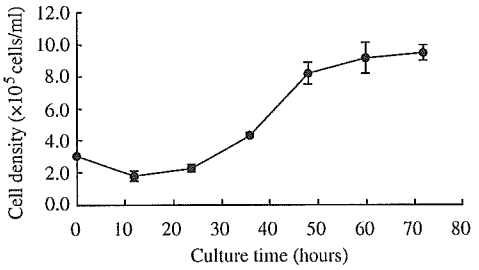

Fig. 7. Time course of cell density of FLAG-tagged prestin-expressing CHO cells cultured in CHO-S-SFM II medium. Cell density was counted with a hemocytometer every 12 h. Error bars show ± SD ($n = 4$).

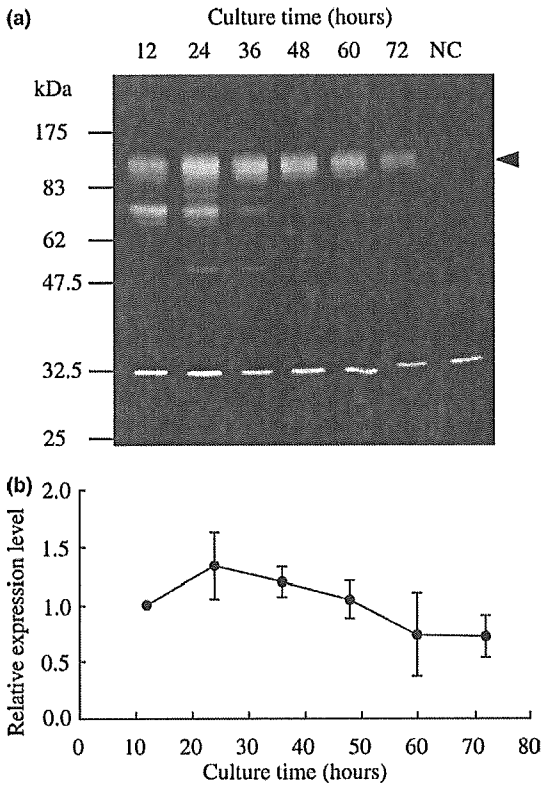

Fig. 8. Expression level of FLAG-tagged prestin in CHO cells cultured in CHO-S-SFM II medium. (a) Representative result of Western blot analysis. Cells (5×10^4) harvested every 12 h during the culture were loaded. Arrow indicates the prestin bands. NC: untransfected CHO cells. (b) Time course of the relative expression level of prestin. The expression levels in the cells at different points of time relative to that in the cells cultured 12 h after passage were evaluated from the luminescence intensity of Western blot bands. Error bars show ± SD ($n = 4$).

be expressed in CHO cells. As the composition and constitution of the membrane of *E. coli* are generally recognized to be quite different from those of the mammalian plasma membrane, we did not expect prestin to be expressed in the membrane of *E. coli*. We alternatively expected that prestin, which is a hydrophobic membrane protein, would be expressed as an inclusion body using the pET28b expression vector or as a solubilized protein fused with hydrophilic MBP using the pMAL-c2 expression vector. Contrary to expectations, however, prestin was not expressed in these cells at all. It is presumed that prestin is toxic for *E. coli*.

In our Western blot analysis (Fig. 1), when the baculovirus expression system was used, a band around 65 kDa and some weak bands below that were detected in transfected cells, while no band was detected in untransfected cells. The band around 65 kDa represents prestin and the other lighter bands are likely to represent fragments of prestin. On the other hand, when the CHO expression system was used, a band around 90 kDa representing prestin was detected in transfected cells. Bands around 30 kDa detected in both transfected CHO cells and untransfected CHO cells may have resulted from nonspecific binding of antibodies. The difference between the band around 90 kDa, characterized by broadness and brightness, detected in CHO cells and the band around 65 kDa, characterized by sharpness, detected in Sf9 cells suggests that prestin expressed in CHO cells is glycosylated while that in Sf9 insect cells is not. As prestin expressed in CHO cells is modified by different lengths of carbohydrate chains, prestin expressed in CHO cells is heavier than that in Sf9 cells and varies in molecular weight. As a result, the position of the band detected in CHO cells is higher than that detected in Sf9 cells, and the band detected in CHO cells is broad. Stabilization of prestin would also be realized by glycosylation, which may lead to a high level of expression of prestin in CHO cells. As a result, the band detected in CHO cells was brighter than that detected in Sf9 cells. The idea that prestin is glycosylated in CHO cells agrees with a glycosylation study of prestin reported by Matsuda et al. (2004).

In our experimental results, prestin was not expressed in *E. coli* at all and only slightly expressed in insect cells. However, since few attempts were made to express prestin in insect cells and bacterial cells, there is a possibility that it could be expressed in such cells using other host vector systems. Even though there are other possibilities to obtain prestin, we adopted the CHO cell expression system because prestin was well expressed in CHO cells.

Transfected cell lines were obtained by limiting dilution cloning, and GFP was stably expressed for over 4 months in these cell lines. As the prestin gene and the GFP gene are transcribed into sequential mRNA when the constructed expression vector is used, stable expression of prestin may be achieved in these cell lines. In fact, according to the results of immunofluorescence experiments shown in Fig. 2, it was confirmed that FLAG-tagged prestin was stably expressed in the generated cell line after subculturing for 4 months. As the same expression vector was applied, it was anticipated that wild-type prestin was also stably expressed in the

generated cell line. We therefore considered that the stable prestin-expressing cell lines have been established using transfected CHO cells.

The electrophysiological properties of the OHCs measured in this study agree with those of OHCs reported by Huang and Santos-Sacchi (1993), and the electrophysiological properties of prestin-expressing CHO cells, which were subcultured for over 4 months and measured in this study, agree with those of transiently prestin-expressing CHO cells reported by Ludwig et al. (2001). As both the established wild-type prestin-expressing and FLAG-tagged prestin-expressing cell lines exhibited bell-shaped nonlinear membrane capacitance fitted to Eq. (4), similar to prestin in the OHCs, wild-type prestin and FLAG-tagged prestin expressed in the established cell lines have activity. Moreover, as there were no significant differences between the electrophysiological properties of wild-type prestin-expressing cells and those of FLAG-tagged prestin-expressing cells, it is concluded that the FLAG-tag does not interfere with the function of prestin (Table 1). FLAG-tagged prestin can therefore be applied to the study of prestin.

Nonlinear membrane capacitance was not obtained in about half of the transfected cells. The reason for this result may have been individual differences in the expression level of prestin in the transfected cells. When the expression level of prestin was low, it was difficult to obtain nonlinear membrane capacitance which fitted Eq. (4) with a correlation coefficient of $R \geqslant 0.98$ because the measured membrane capacitance was affected by measurement noise. If measurement noise were decreased, more cells would show nonlinear capacitance. Although about half of the transfected cells do not show nonlinear capacitance, i.e., the expression level of prestin in some cells is low, it does not interfere with obtaining prestin from those cells.

The expression level of prestin in the established cell line was then estimated using the obtained linear capacitance, C_{lin}, and the maximum charge transfer, Q_{max}. As Q_{max} indicates the total amount of charge carried by all prestin in the plasma membrane and e is electron charge, which is presumed to equal the charge carried by one prestin molecule, the number of prestin molecules in the cell is given by Q_{max}/e. As C_{lin} expressed in picofarads indicates the total capacitance of the plasma membrane of the cell, and the membrane capacitance of the cell per unit surface area is known to be 0.01 pF/μm^2 (Neher and Marty, 1982), the surface area of the cell is expressed by $C_{\mathrm{lin}}/0.01$ μm^2. The expression level of prestin per unit surface area, i.e., charge density, of the cell can therefore be obtained with

$$\text{Charge density} = \frac{Q_{\mathrm{max}}}{e} \Big/ \frac{C_{\mathrm{lin}}}{0.01}. \tag{6}$$

The charge density of the 20 measured wild-type prestin-expressing CHO cells and 19 measured FLAG-tagged prestin-expressing CHO cells were determined to be 246 ± 125 and 255 ± 88 μm^{-2}, respectively (Table 1). The charge densities of established cell lines are lower than the average density of OHCs, which is 6830 μm^{-2} as obtained in this study or 7500 μm^{-2} as reported by Huang and Santos-Sacchi (1993). The charge densities are also lower than that of transiently prestin-expressing TSA201 cells, reported to be 5360 μm^{-2} by Zheng et al. (2000). Although the expression levels were 1/20–1/35 of those in OHCs and TSA201 cells, the stable expression of prestin in the established cell lines is an advantage.

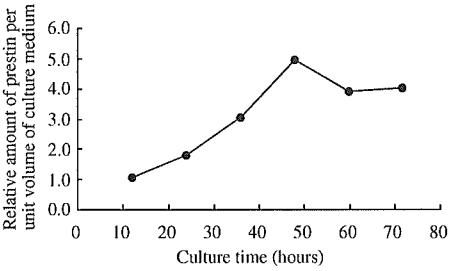

Fig. 9. Time course of the relative values of the amount of prestin in unit volume of culture medium. The amount of prestin included in unit volume of culture medium was the result of multiplication of the cell density by the relative expression level. Values were normalized to the value of 12 h after passage.

To obtain prestin efficiently, the optimal culture conditions for an established cell line was considered. Generally, suspension culture is advantageous for obtaining a large number of cells because cell number per unit volume of medium can be raised by use of a three-dimensional culture rather than a monolayer culture, and culture procedures are manageable. The established FLAG-tagged prestin-expressing cells were therefore cultured in CHO-S-SFM II medium to achieve growth of suspension cells. The cells cultured as suspension cells also exhibited a bell-shaped nonlinear membrane capacitance, i.e., prestin expressed in suspension cells has activity. When prestin is researched at the molecular level, the percentage of prestin in total proteins expressed in the cells, which is shown in Fig. 8(b), is an important factor because impurities interfere with the experimental procedure. The amount of prestin per unit volume of culture medium, which is shown in Fig. 9, is another important factor for efficient acquisition. This is obtained by multiplication of the cell density (Fig. 7) by the expression level (Fig. 8(b)). Fig. 8(b) demonstrates that the variation of the relative expression level is relatively small (from 0.7 to 1.3). By contrast, the relative amount of prestin per unit volume of culture medium increased from 1.0 up to 4.9 at 48 h after passage, and then decreased. From these results, it is concluded that cells should be harvested around 48 h after passage to efficiently obtain prestin.

5. Conclusions

In this study, to obtain a large amount of prestin, an expression system for prestin was constructed. The conclusions are as follows:

1. Prestin was expressed in mammalian cells, but not in *E. coli* nor in insect cells.
2. Prestin-expressing cell lines were generated by limiting dilution cloning. In these cell lines, although the expression levels were 1/20–1/35 of those in OHCs and of those in TSA201 cells transiently expressing prestin, prestin was expressed stably in the generated cell lines.
3. To obtain prestin efficiently, cells should be grown as suspension cells using CHO-S-SFM II medium, and be harvested at approximately 48 h after passage.

Acknowledgements

This work was supported by a grant from the Human Frontier Science Program, by a Health and Labor Science Research Grant from the Ministry of Health, Labor and Welfare of Japan, and by Grant-in-Aid for Scientific Research on Priority Areas 15086202 from the Ministry of Education, Culture, Sports, Science and Technology of Japan.

References

Ashmore, J.F., 1987. A fast motile response in guinea-pig outer hair cells: the cellular basis of the cochlear amplifier. J. Physiol. 388, 323–347.

Avgerinos, G.C., Drapeau, D., Socolow, J.S., Mao, J., Hsiao, K., Broeze, R.J., 1990. Spin filter perfusion system for high density cell culture: production of recombinant urinary type plasminogen activator in CHO cells. Biotechnology 8, 54–58.

Brownell, W.E., Bader, D., Ribaupierre, Y., 1985. Evoked mechanical responses of isolated cochlear outer hair cells. Science 227, 194–196.

Dallos, P., 1992. The active cochlea. J. Neurosci. 12, 4575–4585.

Forge, A., 1991. Structural features of the lateral walls in mammalian cochlea outer hair cells. Cell Tissue Res. 265, 473–485.

Frolenkov, G.I., Mammano, F., Belyantseva, I.A., Coling, D., Kachar, B., 2000. Two distinct Ca^{2+}-dependent signaling pathways regulate the motor output of cochlear outer hair cells. J. Neurosci. 20, 5940–5948.

Huang, G., Santos-Sacchi, J., 1993. Mapping of the distribution of the outer hair cell motility voltage sensor by electrical amputation. Biophys. J. 65, 2228–2236.

Kachar, B., Brownell, W.E., Altschuler, R., Fex, J., 1986. Electrokinetic shape changes of cochlear outer hair cells. Nature 322, 365–368.

Liberman, M.C., Gao, J., He, D.Z.Z., Wu, X., Jia, S., Zuo, J., 2002. Prestin is required for electromotility of the outer hair cell and for the cochlear amplifier. Nature 419, 300–304.

Ludwig, J., Oliver, D., Frank, G., Klöcker, N., Gummer, A.W., Fakler, B., 2001. Reciprocal electromechanical properties of rat prestin: the motor molecule from rat outer hair cells. Proc. Natl. Acad. Sci. USA 98, 4178–4183.

Matsuda, K., Zheng, J., Du, G.G., Klöcker, N., Madison, L.D., Dallos, P., 2004. N-linked glycosylation sites of the motor protein prestin: effects on membrane targeting and electrophysiological function. J. Neurochem. 89, 928–938.

Neher, E., Marty, A., 1982. Discrete changes of cell membrane capacitance observed under conditions of enhanced secretion in bovine adrenal chromaffin cells. Proc. Natl. Acad. Sci. USA 79, 6712–6716.

Oliver, D., He, D.Z.Z., Klöcker, N., Ludwig, J., Schulte, U., Waldegger, S., Ruppersberg, J.P., Dallos, P., Fakler, B., 2001. Intracellular anions as the voltage sensor of prestin, the outer hair cell motor protein. Science 292, 2340–2343.

Santos-Sacchi, J., 1991. Reversible inhibition of voltage-dependent outer hair cell motility and capacitance. J. Neurosci. 11, 3096–3110.

Santos-Sacchi, J., Dilger, J.P., 1988. Whole cell currents and mechanical responses of isolated outer hair cells. Hear. Res. 35, 143–150.

Santos-Sacchi, J., Shen, W., Zheng, J., Dallos, P., 2001. Effects of membrane potential and tension on prestin, the outer hair cell lateral membrane motor protein. J. Physiol. 531, 661–666.

Wu, X., Gao, J., Guo, Y., Zuo, J., 2004. Hearing threshold elevation precedes hair-cell loss in prestin knockout mice. Mol. Brain Res. 126, 30–37.

Zenner, H.P., 1986. Motile responses in outer hair cells. Hear. Res. 22, 83–90.

Zheng, J., Long, K.B., Shen, W., Madison, L.D., Dallos, P., 2001. Prestin topology: localization of protein epitopes in relation to the plasma membrane. NeuroReport 12, 1929–1935.

Zheng, J., Shen, W., He, D.Z.Z., Long, K.B., Madison, L.D., Dallos, P., 2000. Prestin is the motor protein of cochlear outer hair cells. Nature 405, 149–155.

Effects of Mutation in the Conserved GTSRH Sequence of the Motor Protein Prestin on Its Characteristics*

Shun KUMANO**, Koji IIDA**, Michio MURAKOSHI**,
Naoyuki NAITO**, Kouhei TSUMOTO***, Katsuhisa IKEDA****,
Izumi KUMAGAI†, Toshimitsu KOBAYASHI†† and Hiroshi WADA**

Prestin is a motor protein responsible for the outer hair cell (OHC) electromotility which amplifies the vibration of the organ of Corti in the inner ear. Identification of the functional significance of particular amino acids is necessary to characterize prestin. In this study, an attempt was made to clarify the role of the GTSRH sequence at positions 127–131 in prestin conserved in six proteins of the solute carrier (SLC) 26 family of which prestin is a member. To elucidate what role that sequence plays in the characteristics of prestin, mutations were introduced into the sequence and the characteristics of the constructed point mutants were investigated by Western blotting, immunofluorescence experiments and the whole-cell patch-clamp technique. The localization of T128A was altered, the anion transport function of H131A and that of S129T were lost and such functions of G127A, T128A, S129A and R130A declined. These results suggest that the GTSRH sequence plays an important role in the localization of prestin, as well as in its anion transport function.

Key Words: Seeing and Hearing Mechanism, Biomechanics, Measurement, Acoustic, Sound, Outer Hair Cell, Motor Protein, Prestin, Mutagenesis

1. Introduction

Outer hair cells (OHCs) in the mammalian organ of Corti elongate and contract in response to the change of their membrane potential, this OHC motility being generally referred to as electromotility[1]-[3]. The electromotility amplifies the vibration of organ of Corti (Fig. 1) and this amplification mechanism realizes the high sensitivity and sharp tuning of the auditory system[4]. It is inferred that the OHC is a direct voltage-to-force converter without dependence on ATP and can operate at microsecond rates[3]. The OHC motility is accompanied by a charge movement that can be recorded as nonlinear capacitance

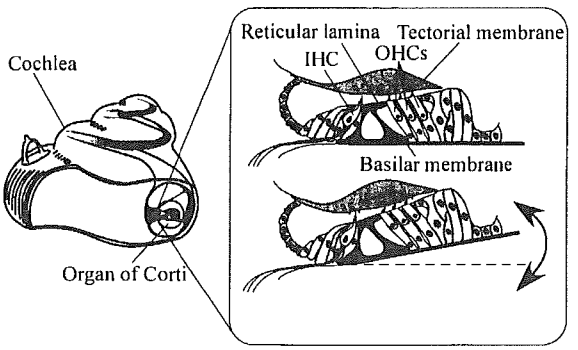

Fig. 1 Schematic of the cochlea and a cross section of the organ of Corti. When the basilar membrane is vibrated, shear motion between the tectorial membrane and the reticular lamina is evoked. Due to the deflection of the stereocilia of the IHC and OHCs, intracellular depolarization evoked by cation influx causes auditory nerve fiber activation of the IHC and simultaneously, the motile response applying force to the basilar membrane is produced in OHCs.

* Received 10th June, 2005 (No. 05-4072)
** Department of Bioengineering and Robotics, Tohoku University, 6–6–01 Aoba-yama, Sendai 980–8579, Japan. E-mail: wada@cc.mech.tohoku.ac.jp
*** Department of Medical Genome Sciences, The University of Tokyo, 5–1–5 Kashiwanoha, Kashiwa 277–8561, Japan
**** Department of Otorhinolaryngology, Juntendo University School of Medicine, 2–1–1 Hongo, Bunkyo-ku, Tokyo 113–8431, Japan
† Department of Biomolecular Engineering, Tohoku University, 6–6–07 Aoba-yama, Sendai 980–8579, Japan
†† Department of Otolaryngology, Head and Neck Surgery, Tohoku University Graduate School of Medicine, 1–1 Seiryo-machi, Sendai 980–8575, Japan

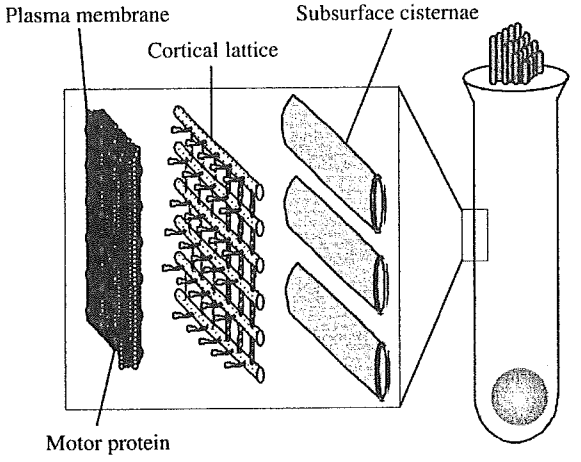

Fig. 2 Lateral wall of the OHC. The OHC lateral wall has a unique trilaminate structure: the outermost plasma membrane, the cortical lattice and the innermost subsurface cisternae. The motor protein is thought to be embedded in the plasma membrane.

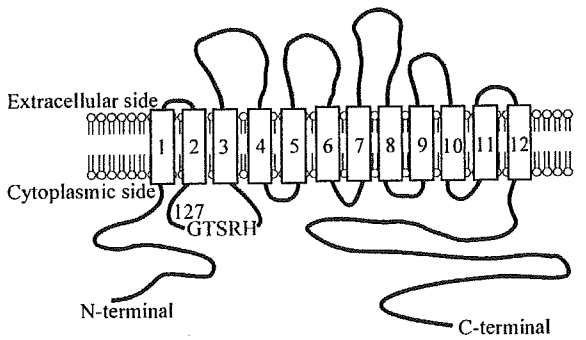

Fig. 3 Predicted membrane topology of prestin. It is considered that prestin has 12 transmembrane domains and that the N-terminus and C-terminus of prestin are located in the cytoplasm[9),(16)]. The GTSRH sequence is at position 127–131 of prestin. The membrane topology was drawn based on the Swiss-Prot/TrEMBL database.

(NLC)[5]. The source of the somatic length change of the OHCs is considered to be the conformational changes of a motor protein in the lateral plasma membrane of the OHCs[6),(7)] (Fig. 2). In 2000, this motor protein was identified in the gerbil cochlea and termed prestin[8].

As shown by amino acid sequence analyses, prestin consists of 744 amino acids with a molecular weight of about 81.4 kDa and is a member of the solute carrier (SLC) 26 family which transports anions through the cell membrane[8] (Fig. 3). Mammalian cells transfected with prestin exhibit electromotility and NLC[8),(9)]. By contrast, OHCs isolated from prestin knockout mice lack electromotility[10]. From these results, prestin is believed to be the motor protein in the OHCs. However, the mechanism by which prestin functions has been unknown. For further clarification of that mechanism, it is necessary to elucidate the role of each amino acid of prestin.

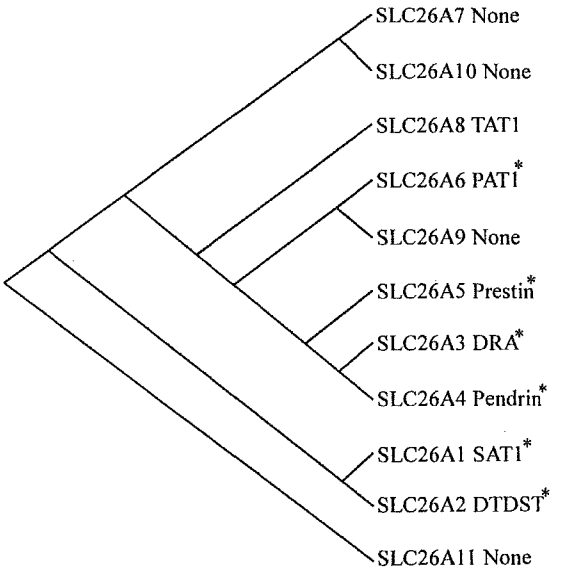

Fig. 4 Dendrogram of the SLC26 family. Human orthologs were used to generate a dendrogram with CLUSTALW. The GTSRH sequence is conserved in six proteins of the SLC26 family, which are indicated by asterisks. The amino acid sequences of the SLC26 family were obtained from the Swiss-Prot/TrEMBL database.

The GTSRH sequence of amino acids at positions 127–131 was completely conserved in six proteins of the SLC26 family (Fig. 4). In the case of pendrin, which is a member of the SLC26 family, substitution of threonine for serine in the GTSRH sequence is known to lead to syndromic hearing impairment[11]. It is therefore likely that the GTSRH sequence is crucial for the SLC26 family. In this study, to clarify the role of the GTSRH sequence in the characteristics of prestin, alanine was substituted for glycine, threonine, serine, arginine and histidine individually and threonine was substituted for serine. Wild-type (WT) prestin and point mutants were expressed in human embryonic kidney (HEK) 293 cells. The expressions and localizations of WT prestin and the point mutants in HEK293 cells were then investigated by Western blotting and immunofluorescence experiments. Additionally, the membrane capacitance, which is an indicator of the anion transport function, of WT prestin and those of the point mutants were recorded by the whole-cell patch-clamp technique. By comparing the results for the WT prestin with those for the point mutants, the roles of the GTSRH sequence in the characteristics of prestin were examined.

2. Materials and Methods

2.1 Site-directed mutagenesis

The GTSRH sequence at positions 127–131 was altered, i.e., alanine was substituted for glycine, threonine, serine, arginine and histidine individually and thre-

Table 1 Primers used for site directed mutagenesis

Name	Sequence
5′ flanking forward	5′-CGGGATCCATGGATCATGCCGAAGAAAAATG-3′
3′ flanking reverse	5′-GGAATTCTTATGCCTCGGGTGTGGTGG-3′
3′ flanking FLAG reverse	5′-CCGCTCGAGTGCCTCGGGTGTGGTGGG-3′
G127A forward	5′-CTGTTTCTTTGCGACCTCCAGAC-3′
G127A reverse	5′-GTCTGGAGGTCGCAAAGAAACAG-3′
T128A forward	5′-GTTTCTTTGGGGCCTCCAGACAC-3′
T128A reverse	5′-GTGTCTGGAGGCCCCAAAGAAAC-3′
S129A forward	5′-CTTTGGGACCGCCAGACACATATC-3′
S129A reverse	5′-GATATGTGTCTGGCGGTCCCAAAG-3′
R130A forward	5′-CTTTGGGACCTCCGCACACATATCTATAG-3′
R130A reverse	5′-CTATAGATATGTGTGCGGAGGTCCCAAAG-3′
H131A forward	5′-GGGACCTCCAGAGCCATATCTATAGG-3′
H131A reverse	5′-CCTATAGATATGGCTCTGGAGGTCCC-3′
S129T forward	5′-CTTTGGGACCACCAGACACATATC-3′
S129T reverse	5′-GATATGTGTCTGGTGGTCCCAAAG-3′

onine was substituted for serine, resulting in six point mutants with the following sequences: ATSRH, GASRH, GTARH, GTSAH, GTSRA and GTTRH. These point mutants were constructed using overlap extension PCR with gerbil prestin cDNA inserted into the expression vector pIRES-hrGFP-1a (Stratagene, La Jolla, CA) as a template. Two separate PCRs were carried out with one flanking primer and one mutagenic primer which contained at least 23 bp homologous to that of other mutagenic primer (Table 1). For example, to construct the G127A mutant, one reaction solution contained a 5′ flanking forward primer and a G127A reverse primer, and the other solution contained a 3′ flanking reverse primer and a G127A forward primer. The two PCR products were purified from agarose gel after DNA electrophoresis, mixed together, and assembled by a primerless PCR. The assembled products were amplified with the two flanking primers. The resulting PCR product was gel purified and digested with *BamH*I and *EcoR*I (New England Biolabs, Beverly, MA). Digested products were ligated into *BamH*I and *EcoR*I sites of the expression vector.

To visualize prestin by using antibodies in Western blotting and immunofluorescence experiments, FLAG-tagged mutant prestin genes were constructed. The FLAG-tag sequence is downstream of the *Xho*I site in the pIRES-hrGFP-1a. Hence, to insert a mutant prestin gene between the *BamH*I and *Xho*I sites of the expression vector, a 3′ flanking FLAG reverse primer lacking the stop codon of prestin and having the *Xho*I site was used in overlap extension PCR. The resulting amplified products were gel purified and digested with *BamH*I and *Xho*I (New England Biolabs). Digested products were ligated into *BamH*I and *Xho*I sites of the expression vector. Each mutation was verified by an automated DNA sequencer (Applied Biosystems, Foster City, CA).

2.2 Cell culture and transfection

The difference of the characteristics between WT prestin and the point mutants can be clarified by using a cell line which does not express prestin. As the efficiencies of transfection and protein expression of HEK293 cells are high, this cell line was used for following experiments. HEK293 cells were cultured in RPMI-1640 medium with 10% fetal bovine serum, 100 U penicillin/mL and 100 μg streptomycin/mL at 37°C with 5% CO_2. One day before transfection, HEK293 cells were plated in 35-mm culture dishes. Constructed expression vectors were transfected into HEK293 cells using LipofectAMINE 2000 Reagent (Invitrogen, Rockville, MD) according to the manufacturer's instructions. As the transfected cells expressed green fluorescent protein (GFP) due to the GFP gene inserted into the expression vector, the introduction of the expression vectors was confirmed by GFP observation.

2.3 Western blotting

To confirm the expression of FLAG-tagged point mutants and the molecular weight of the expressed proteins, Western blotting was performed. The transiently transfected cells were dissolved in SDS sample buffer at a concentration of 1×10^5 cells/10 μL. After boiling for 5 min at 100°C, 10 μL of the cell lysates were electrophoresed on 10% polyacrylamide gel. Separated proteins in an SDS-PAGE were transferred to nitrocellulose membranes (Hybond-ECL, Amersham Biosciences, Uppsala, Sweden). The membranes were blocked by 5% skim milk in PBS containing 0.05% Tween20 (PBS-T). After blocking and PBS-T washing, the membranes were incubated with anti-FLAG mouse monoclonal antibody (Sigma-Aldrich, St. Louis, MO) in PBS-T. After incubation for 30 min at room temperature, the membranes were washed with PBS-T. The membranes were then incubated with HRP-conjugated anti-mouse IgG antibody